Exploring Protein-Protein Ligation Approaches for the Cytosolic Delivery of Antigens Using AIP56

Bruno Pinheiro , Ana C. Moura , Pedro N. Oliveira , Jorge E. Azevedo , Ana do Vale , Nuno M.S. dos Santos *

Posted Date: 5 February 2025

doi: 10.20944/preprints202502.0284.v1

Keywords: AB toxins; biologics; cytosolic delivery; protein-protein fusion

Article

Exploring Protein-Protein Ligation Approaches for the Cytosolic Delivery of Antigens Using AIP56

Bruno Pinheiro [1,2,3], Ana C. Moura [1,2], Pedro N. Oliveira [4], Jorge E. Azevedo [4,5,6], Ana do Vale [1,2] and Nuno M.S. dos Santos [1,2,*]

[1] Fish Immunology and Vaccinology, Instituto de Investigação e Inovação em Saúde (i3S), Universidade do Porto, Porto, Portugal
[2] Fish Immunology and Vaccinology, Instituto de Biologia Molecular e Celular (IBMC), Universidade do Porto, Porto, Portugal
[3] Doctoral Program in Molecular and Cell Biology (MCBiology), Instituto de Ciências Biomédicas Abel Salazar (ICBAS), Universidade do Porto, Porto, Portugal
[4] Instituto de Ciências Biomédicas Abel Salazar (ICBAS), Universidade do Porto, Porto, Portugal
[5] Organelle Biogenesis and Function, Instituto de Investigação e Inovação em Saúde (i3S), Universidade do Porto, Porto, Portugal
[6] Organelle Biogenesis and Function, Instituto de Biologia Molecular e Celular (IBMC), Universidade do Porto, Porto, Portugal
* Correspondence: nsantos@i3s.up.pt

Abstract: Background/Objectives: The intracellular delivery of biologics, particularly large cargoes like proteins, remains a challenge in biotechnology and biomedicine. The modular structure of well-characterized AB toxins allows different cargoes to be grafted, creating a target-specific biotechnological tool capable of cytosolic delivery. **Methods**: In this study, we employed protein-protein fusion strategies - SpyCatcher003, SnoopCatcher, and SnoopLigase - to generate chimeras between the delivery region of AIP56 ($AIP56^{L258\text{-}N497}$) and β-lactamase and performed functional delivery assays. **Results**: The chimeras were successfully obtained using these strategies and *in vitro* β-lactamase activity assays confirmed the catalytic activity of the chimeras. Importantly, we show that the chimera $Bla^{L19\text{-}W286}$::$SnoopAIP56^{L258\text{-}N497}$ delivered β-lactamase into the cytosol of J774.A1 macrophages. **Conclusions**: AIP56 delivery region transporting other cargo directly to the cytosol of antigen-presenting cells might be a promising platform for antigen delivery. This study highlights the potential of protein-protein fusion strategies to create versatile, antigenically distinct toxin-based delivery systems for therapeutic applications.

Keywords: AB toxins; biologics; cytosolic delivery; protein-protein fusion

1. Introduction

The use of biopharmaceuticals (biologics) for replacement therapy, vaccines or as agonists/antagonists has a huge potential in therapeutic and prophylactic strategies. Indeed, the demand for biologics has grown steadily in recent years, with a market size estimated to reach 532.2 billion USD by 2027 [1]. The advantages of using biologics are manifold and include their high potency and specificity, their diverse molecular targets and their lower toxicity and tissue accumulation when compared with traditional small-drug molecules [2,3]. However, delivering protein-based biologics into the cytosol of eukaryotic cells remains a major challenge, as they cannot be readily transported across the lipid membrane of the cells due to their usually large size, polarity, and complexity. This limitation hinders the full potential of biologics and constrains their use to extracellular targets only. This is a particular relevant draw-back for vaccination strategies, because the delivery of antigens to the cytosol of antigen-presenting cells (APCs) is a major goal to activate

 doi:10.20944/preprints202502.0284.v1

specific cytotoxic T lymphocyte (CTL) responses and achieve effective vaccination against cancer or intracellular pathogens, as notably exemplified by anti-cancer RNA-based vaccines [4] and the RNA- and viral-based vaccines currently used to fight COVID-19 [5]. In addition, current vehicles for delivering drugs to the cell cytosol, such as virus-like particles (VLPs) [6], cell-penetrating peptides (CPPs) [7,8] or nanoparticles (NPs) [9], lack selectivity to target specific cells and tissues, have poor endosomal escape capacity and limited *in vivo* efficacy [10]. Therefore, delivery tools that could efficiently and safely transport functional biological molecules into the cytosol of specific cells are a pressing need [10,11].

A promising solution to overcome this challenge may be provided by bacterial AB toxins [10,11]. These toxins are remarkably specific and potent virulence factors secreted by bacteria that act on molecular targets inside eukaryotic cells [12]. They generally display a modular structure comprising two distinct components: component A, containing an enzymatic activity towards molecules with crucial function in eukaryotic cells; and component B, containing a receptor-binding domain or region conferring cell specificity, and a translocation domain or region that assists the translocation of the enzymatic moiety into the cytosol [12]. Components A and B can be encoded in a single gene (i.e., single chain toxins), or coded by independent genes yielding multicomponent toxins whose subunits are associated by non-covalent interactions [13,14]. After receptor-mediated endocytosis, AB toxins reach their cytosolic target either directly from the endosomal compartment upon acidic pH-triggered unfolding and pore formation (short-trip toxins), or from the endoplasmic reticulum (ER) after retrograde transport from the endosomal compartment to the ER (long-trip toxins). The modular structure confers to AB toxins advantages as biotechnological tools, since different cargoes can be grafted to them to generate new chimeric molecules with novel properties [10,11,15,16]. Not surprisingly, several AB toxins have already been used to generate useful molecules. For instance, *Pseudomonas* exotoxin A has been engineered as immunotoxins for antitumor therapy, shiga toxin has been engineered for the delivery of cytotoxic drugs in Gb3-positive tumors and both cholera toxin and *Bordetella pertussis* adenylate cyclase (CyaA) toxin were engineered as antigen delivery platforms to promote highly specific immune responses [17–22].

We have been characterizing AIP56 (Apoptosis Inducing Protein of 56 kDa), a single chain AB toxin [23,24] that targets sea bass (*Dicentrarchus labrax*) macrophages [23,25]. AIP56 is secreted by the type 2 secretion system of *Photobacterium damselae* subsp. *piscicida* [26], a Gram-negative bacterium pathogenic for warm water marine fish that causes high economic losses to the aquaculture sector. The toxin has a three-domain organization [27]: (i) a N-terminal catalytic domain that cleaves NF-kB p65 [24]; (ii) a small and structurally simple middle domain involved in pore formation; and (iii) a C-terminal domain involved in receptor-binding and pore formation [24,27]. After binding to a still unknown host cell receptor, AIP56 is endocytosed [25] and, upon endosomal acidification, protonation of pH-sensing residues located at the carboxyl-terminal portion of the catalytic domain promotes conformational changes that lead to membrane insertion and pore formation [27], with consequent translocation of the catalytic domain to the cytosol [28]. Cleavage of cytosolic NF-kB p65 in intoxicated sea bass macrophages leads to their death by post-apoptotic secondary necrosis [23]. Importantly, mouse and human monocytes, macrophages and dendritic cells (DCs) also internalize AIP56 and undergo p65 cleavage [25,29]. Given the tropism of AIP56 for mammalian APCs, which are clinically-relevant cell targets for immunization, this toxin may potentially be used as a platform to deliver antigens into the cytosol of APCs and, in this way, serve as a universal vaccination vector.

We have shown previously that AIP56 is able to transport and efficiently translocate genetically-fused β-lactamase (Bla) into the cytosol of mouse macrophages [30]. However, not all antigens can be genetically coupled to toxin-based delivery platforms, because such fusions are often poorly expressed or unstable/insoluble [10,11,20]. In principle, this limitation can be overcome by using "molecular glues". These ligation systems allow to produce vector and cargo separately in their native forms and fuse them later, allowing fusion of synthetic antigens or antigens that contain lipidic or glycosidic determinants [31–33].

 doi:10.20944/preprints202502.0284.v1

Systems such as SpyCatcher are based on the Ig-like domains of adhesins from *Streptococcus pyogenes* that contain an internal isopeptide bond between a lysine and an aspartate, the synthesis of which is catalyzed by an opposing glutamate (Figure S1a) [34,35]. The Howarth Lab splitted these domains into a short peptide (SpyTag) containing the reactive aspartate (SpyTag) and a small protein partner (SpyCatcher), containing the reactive lysine and the catalyst glutamate. Both parts can be genetically added to proteins that, when mixed together, spontaneously form an irreversible isopeptide bond very rapidly, promoting their fusion [34]. A very similar alternative to SpyCatcher has been developed by the same group from a *Streptococcus pneumoniae* adhesin, named SnoopCatcher. In this version, the tag (SnoopTag) contains a reactive lysine, while its protein partner contains a reactive asparagine and the catalyst glutamate (Figure S1b) [36,37]. By splitting the SnoopCatcher system into a trio, so that the three residues involved in the reaction are located into each unit, they also created the SnoopLigase strategy. An enzyme-like protein that contains the catalyst glutamate (SnoopLigase), promotes the ligation of SnoopTagJr (an improved version of SnoopTag) to a small peptide containing the reactive aspargine (DogTag) (Figure S1b) [38].

In this work, we explored the SpyCatcher003 (improved version of SpyCatcher) [34,39–41], SnoopCatcher [36] and SnoopLigase [38,42] ligation systems to fuse β-lactamase to the delivery region of AIP56 (AIP56$^{L258\text{-}N497}$), and tested the ability of the chimeras to deliver β-lactamase into the cytosol of macrophages as a proof-of-concept for an AIP56-based antigen delivery platform.

Materials and Methods

2.1. Cloning

Plasmids used and generated in this work are listed in Table 1. β-lactamase plasmids were constructed by amplifying the nucleotide sequence encoding Bla$^{L19\text{-}W286}$ from plasmid p327 and cloning it into pET28a NcoI/XhoI restriction sites, in frame with a DNA sequence encoding a flexible glycine-glycine-serine-glycine (GGSG) linker and SnoopTagJr (Bla$^{L19\text{-}W286}$SnoopTagJr) or SpyTag003 (Bla$^{L19\text{-}W286}$SpyTag003), both introduced by PCR, and a C-terminal 6×His-tag. The construct for the genetic chimera Bla$^{L19\text{-}W286}$::AIP56$^{L258\text{-}N497}$ was generated in a previous work [30]. The construct encoding DogTagAIP56$^{L258\text{-}N497}$ was obtained by amplifying the nucleotide sequence encoding AIP56$^{L258\text{-}N497}$ from pET28AIP56H+ [23] and cloning it into the NcoI/XhoI restriction sites of pET28a, in frame with DogTag at the N-terminus (introduced by PCR) and a C-terminal 6×His-tag. To generate constructs encoding SnoopCatcherAIP56$^{L258\text{-}N497}$ and SpyCatcher003AIP56$^{L258\text{-}N497}$, AIP56$^{L258\text{-}N497}$ nucleotide sequence was amplified from pET28AIP56H+ [23] and cloned into the SacI/XhoI restriction sites of pET28a, in frame with a C-terminal 6×His-tag, rendering pET28a_AIP56$^{L258\text{-}N497}$. SnoopCatcher was amplified from pET28a–SnoopCatcher, whereas SpyCatcher003 was amplified from pDEST14-SpyCatcher003. Finally, both sequences were cloned into pET28a_AIP56$^{L258\text{-}N497}$ NcoI/SacI restriction sites rendering pET28a_SnoopCatcherAIP56$^{L258\text{-}N497}$ and pET28a_SpyCatcher003AIP56$^{L258\text{-}N497}$, respectively.

Table 1. Plasmids used in this work.

Plasmid	Purpose	Source/Reference
p327	Template to amplify the coding sequence of Bla$^{L19\text{-}W286}$	A gift from Dr. Panagiotis Papatheodorou, Ulm University
pET28a_Bla$^{L19\text{-}W286}$SnoopTagJr	Expression of Bla$^{L19\text{-}W286}$ in frame with SnoopTagJr and 6x HisTag in the C-terminal	This work
pET28a_Bla$^{L19\text{-}W286}$SpyTag003	Expression of Bla$^{L19\text{-}W286}$ in frame with SpyTag003 and 6x HisTag in the C-terminal	This work

 doi:10.20944/preprints202502.0284.v1

pET28a_Bla$^{L19\text{-}W286}$AIP56$^{L258\text{-}N497}$	Expression of Bla$^{L19\text{-}W286}$ fused to AIP56$^{L258\text{-}N497}$ in frame with a 6x HisTag in the C-terminal	Rodrigues et al, 2019 [30]
pET28a–SnoopCatcher	Template to amplify the coding sequence of SnoopCatcher	Addgene plasmid #72322; Veggiani et al, 2016 [36]
pDEST14-SpyCatcher003	Template to amplify the coding sequence of SpyCatcher003	Addgene plasmid # 133447; Keeble et al, 2019 [41]
pET28AIP56H+	Template to amplify the coding sequence of AIP56$^{L258\text{-}N497}$	do Vale et al, 2005 [23]
pET28a_AIP56$^{L258\text{-}N497}$	Backbone to insert SnoopCatcher/SpyCatcher003 coding sequence in frame with AIP56$^{L258\text{-}N497}$	This work
pET28a_SnoopCatcherAIP56$^{L258\text{-}N497}$	Expression of SnoopCatcher fused to AIP56$^{L258\text{-}N497}$ in frame with a 6x HisTag in the C-terminal	This work
pET28a_ SpyCatcher003AIP56$^{L258\text{-}N497}$	Expression of SpyCatcher003 fused to AIP56$^{L258\text{-}N497}$ in frame with a 6x HisTag in the C-terminal	This work
pET28a_DogTagAIP56$^{L258\text{-}N497}$	Expression of DogTag fused to AIP56$^{L258\text{-}N497}$ in frame with a 6x HisTag in the C-terminal	This work
pET28a–His6-AviTagSnoopLigase	Expression of AviTag fused to SnoopLigase in frame with a 6x HisTag in the N-terminal	Addgene plasmid #105626; Buldun et al [38]

2.2. Recombinant Protein Production and Purification

Bla$^{L19\text{-}W286}$SnoopTagJr and SpyCatcher003AIP56$^{L258\text{-}N497}$ were expressed in *E. coli* BL21 Star (DE3). Bla$^{L19\text{-}W286}$SpyTag003 was expressed in *E. coli* SoluBL21 (DE3). Bla$^{L19\text{-}W286}$::AIP56$^{L258\text{-}N497}$, SnoopCatcherAIP56$^{L258\text{-}N497}$ and DogTagAIP56$^{L258\text{-}N497}$ were expressed in *E. coli* Rosetta (DE3). AviTagSnoopLigase was expressed in BL21-Codon Plus (DE3).

E. coli competent cells were transformed and cultured at 37 °C in 1 L of Luria Bertani (LB) broth with shaking (200 rpm). Protein expression was induced at OD_{600} ~0.6 by adding 0.5 mM Isopropyl β-D-1-thiogalactopyranoside (IPTG) and carried out at 17 °C for 20 h, except for Bla$^{L19\text{-}W286}$::AIP56$^{L258\text{-}N497}$ and AviTagSnoopLigase, which were expressed for 4 h at 17 °C or 37 °C, respectively. For protein purification, bacterial cells were harvested by centrifugation (3200 g, 30 min, 4 °C) and resuspended in 40 mL of 50 mM Tris-HCl pH 8.0, 300 mM NaCl, or 20 mM Tris-HCl pH 8.0, 200 mM NaCl, 5% (v/v) glycerol in the case of Bla$^{L19\text{-}W286}$::AIP56$^{L258\text{-}N497}$ [30]. Bacteria were lysed by sonication and centrifuged (35000g, 30 min, 4 °C). Recombinant proteins were purified from the supernatant using nickel-agarose beads by gravity-flow chromatography, followed by size-exclusion chromatography (Superose 12 10/300 GL). Recombinant proteins integrity and purity were analyzed by SDS-PAGE and Coomassie-blue R-250 staining.

 doi:10.20944/preprints202502.0284.v1

2.3. Determination of Recombinant Protein Concentration

The concentration of recombinant proteins was assessed by measuring absorbance at 280 nm using a NanoDrop 1000 and/or NanoDrop One (Thermo Fisher Scientific) considering the extinction coefficient and the molecular weight determined using the ProtParam tool available at https://web.expasy.org/protparam/.

2.4. In Vitro Fusion Reactions and Complex Purification

SpyTag003-SpyCatcher003: The reaction between Bla$^{L19\text{-}W286}$SpyTag003 and SpyCatcher003AIP56$^{L258\text{-}N497}$ was tested at 4 °C and 25 °C using 1:1, 2:1 and 5:1 (1 unit equals 10 μM) molar ratios in PBS (final volume of 100 μL). After mixing the two proteins, aliquots were removed immediately (0 h) or after 1, 2, 4, 8 and 24 h incubation, and subjected to SDS-PAGE. The best condition (4 h incubation, 25 °C, molar ratio 5:1) was upscaled to 500 μL and the generated Bla$^{L19\text{-}W286}$::SpyAIP56$^{L258\text{-}N497}$ chimera purified by size-exclusion chromatography (Superdex 75 10/300 GL) in 50 mM Tris-HCl pH 8.0, 300 mM NaCl. The reaction of Bla$^{L19\text{-}W286}$SpyTag003 with SpyCatcher003AIP56$^{L258\text{-}N497}$ resulted in three peaks. Fractions from the peaks were collected and analyzed by SDS-PAGE. Bla$^{L19\text{-}W286}$::SpyAIP56$^{L258\text{-}N497}$ chimera was collected form the second peak, with minimal contamination from single reactants.

SnoopTagJr-SnoopCatcher: The reaction between Bla$^{L19\text{-}W286}$SnoopTagJr and SnoopCatcher003AIP56$^{L258\text{-}N497}$ was tested at 17 °C and 25 °C and 1:1, 2:1 and 1:2 molar ratios in PBS (final volume of 100 μL). Aliquots of the reaction were removed immediately after mixing the proteins (0 h) or after 1, 2, 4, 6, 8, 12 and 24 h incubation, and subjected to SDS-PAGE. The best condition (24 h incubation, 25 °C, molar ratio 2:1) was upscaled to 500 μL and the generated Bla$^{L19\text{-}W286}$::SnoopAIP56$^{L258\text{-}N497}$ chimera purified by size-exclusion chromatography in 50 mM Tris-HCl pH 8.0, 300 mM NaCl (Superose 12 10/300 GL). Conjugation of Bla$^{L19\text{-}W286}$SnoopTagJr and SnoopCatcherAIP56$^{L258\text{-}N497}$ resulted in two peaks. Fractions were collected and analyzed by SDS-PAGE. Bla$^{L19\text{-}W286}$::SnoopAIP56$^{L258\text{-}N497}$ chimera was collected from the first peak, with minimal contamination from single reactants.

SnoopTagJr-DogTag-SnoopLigase: The reaction between Bla$^{L19\text{-}W286}$SnoopTagJr, DogTagAIP56$^{L258\text{-}N497}$ and AviTagSnoopLigase was tested at 4 °C, 17 °C and 25 °C and 1:1:1, 1:2:2, 2:2:1, 2:1:2 molar ratios in 50 mM Tris-Borate pH 8.0, 10% (v/v) glycerol (final volume of 100 μL). Aliquots of the reaction were removed immediately after mixing the proteins (0 h) or after 3, 6, 9, 12, 24, 30, 36 and 48 h incubation, and subjected to SDS-PAGE. To purify the Bla$^{L19\text{-}W286}$::DogAIP56$^{L258\text{-}N497}$ chimera non-covalently bound to AviTagSnoopLigase , the best condition (36 h incubation, 4 °C, molar ratio 2:2:1) was upscaled to 500 μL and the generated Bla$^{L19\text{-}W286}$::DogAIP56$^{L258\text{-}N497}$+AviTagSnoopLigase purified by size-exclusion chromatography (Superose 12 10/300 GL, GE Healthcare) in 50mM Tris pH8.0, 300mM NaCl and then dialyzed to 50 mM Tris-Borate pH 8.0, 10% (v/v) glycerol. After Bla$^{L19\text{-}W286}$SnoopTagJr and DogTagAIP56$^{L258\text{-}N497}$ conjugation by AviTagSnoopLigase, two main peaks were observed. Fractions were collected and analyzed by SDS-PAGE. Bla$^{L19\text{-}W286}$::DogAIP56$^{L258\text{-}N497}$ non-covalently bound to AviTagSnoopLigase, corresponding to the first peak, was collected with minimal contamination from single reactants.

Densitometric analysis of complex formation at each time point was performed using Fiji Software. Briefly, pixel intensity profiles for each time point were plotted and the value obtained at time point 0 h was subtracted to eliminate background effects and/or contaminants.

2.5. Nitrocefin Cleavage Assay

The β-lactamase activities of the proteins were assessed *in vitro* by measuring the linear rate of change in absorbance at 480 nm of nitrocefin, after catalysis. For this, 5 mg of nitrocefin (484400, Merck) were dissolved in 500 μL of DMSO to obtain an 8 mM stock solution. The working solution (0.4 mM), obtained by diluting the stock solution in 100 mM sodium phosphate buffer pH 7.4, was aliquoted and stored at −20 °C, protected from light. For the assay, 20 μM of nitrocefin was mixed

 doi:10.20944/preprints202502.0284.v1

with 5 nM of each protein in a 1 mL plastic cuvette in 100 mM sodium phosphate buffer pH 7.4. The absorbance of the final solution was measured immediately in a Shimadzu UV 2401PC spectrophotometer at 480 nm every 8 s for 30 min. Curves were plotted using GraphPad Prism 8 and the initial rates were defined as the slope from a linear regression of the first 30 s of reaction.

2.6. Sodium Dodecyl-Sulfate Polyacrylamide Gel Electrophoresis (SDS-PAGE)

SDS-PAGE was performed using the Laemmli discontinuous buffer system [43] in 14% polyacrylamide gels. Samples were subjected to heating for 5 min at 95 °C in SDS-PAGE sample buffer (50 mM Tris-HCl pH 8.8, 2% (w/v) SDS, 0.05% (w/v) bromophenol blue, 10% (v/v) glycerol, 2 mM EDTA, and 100 mM DTT) prior to loading.

2.7. Fluorescence Resonance Energy Transfer (FRET) Based Assay

J774A.1 cells were cultured at 37 °C in a humidified chamber and 5% CO_2 atmosphere in Dulbecco's modified Eagle's medium (DMEM) containing 10% (v/v) inactivated fetal bovine serum (FBS). Cells were seeded at a density of 1×10^4 cells per well in ibidi µ-Slide 8 well plates in DMEM containing 10% (v/v) FBS and allowed to attach and grow for 48 h until reaching 60%-70% confluency. The cells were then washed twice with DMEM and incubated with 1 µM of CCF4-AM in Hanks' balanced salt solution (HBSS) for 30 min at room temperature. After washing twice with HBSS, the β-lactamase-containing proteins were added at a final concentration of 25 nM. The cells were kept on ice for 15 min and then incubated at 37 °C for 45 min. Finally, cells were washed twice with Dulbecco's Phosphate Buffered Saline (DPBS) and fixed on ice for 15 min in 4% (wt/vol) paraformaldehyde in DPBS.

Fixed cells were observed with a CFI PL APO LAMBDA 40X/0.95 objective in a Nikon Eclipse Ti-E microscope. The samples were illuminated by a 395 nm LED by a SpectraX light engine using a quad dichroic filter 310DA/FI/TR/CY5-A and emission filters 450/50 and 525/50. Images were acquired with an EMCCD camera iXon ULTRA 888. Three independent experiments were performed, and in each experiment, a minimum of 10 microscopic fields were analyzed per condition.

Ratiometric analysis of images acquired for emission wavelengths (Em) 447 nm and 520 nm, corresponding to the ratio of cleaved CCF4 to uncleaved CCF4, was made using a custom-made ImageJ macro on Fiji software (https://github.com/BMSPinheiro/FIVLab-i3s_macros) [44]. In each experiment, the normalized ratios were calculated by dividing the ratio values in each condition by the average ratio of mock-treated cells.

Normalized ratios from the different treatments were compared using the non-parametric Kruskal-Wallis test, followed by Mann-Whitney test, with Bonferroni correction in GraphPad Prism 8. Differences were considered significant when $p \leq 0.05$.

3. Results

3.1. β-Lactamase Can Be Efficiently Coupled to AIP56 Delivery Region Using Biochemical Approaches

β-lactamase is an enzyme produced by many bacteria [45], with no known mammalian homologues. The enzyme can be fused to the N-terminus or C-terminus of most proteins without compromising its activity and can be detected in eukaryotic cells without much background interference [46–49]. Here, we used three protein-protein ligation systems to fuse β-lactamase to AIP56$^{L258\text{-}N497}$ (middle and receptor-binding domain) as an alternative to genetic fusion.

To obtain Bla$^{L19\text{-}W286}$::AIP56$^{L258\text{-}N497}$ chimeras through protein-protein fusion approaches, each specific tag and protein partner was genetically fused to Bla$^{L19\text{-}W286}$ or AIP56$^{L258\text{-}N497}$, respectively. Specifically, (i) for the SpyCatcher003 reaction (Figure 1a), SpyTag003 was added to the C-terminus of Bla$^{L19\text{-}W286}$ (Bla$^{L19\text{-}W286}$SpyTag003) and the SpyCatcher003 was fused to the N-terminus of AIP56$^{L258\text{-}N497}$ (SpyCatcher003AIP56$^{L258\text{-}N497}$) [41]; (ii) for the SnoopCatcher reaction (Figure 1b), SnoopTagJr was added to the C-terminus of Bla$^{L19\text{-}W286}$ (Bla$^{L19\text{-}W286}$SnoopTagJr), whereas SnoopCatcher was fused to the

 doi:10.20944/preprints202502.0284.v1

N-terminus of AIP56$^{L258\text{-}N497}$ (SnoopCatcherAIP56$^{L258\text{-}N497}$) [36] and; (iii) for the SnoopLigase reaction (Figure 1c), the DogTag was added to the N-terminus of AIP56$^{L258\text{-}N497}$ for subsequent reaction with Bla$^{L19\text{-}W286}$SnoopTagJr, catalyzed by the SnoopLigase [38]. All the proteins were successfully expressed in *Escherichia coli* and purified by Ni-NTA affinity chromatography followed by size-exclusion chromatography (Figure S2).

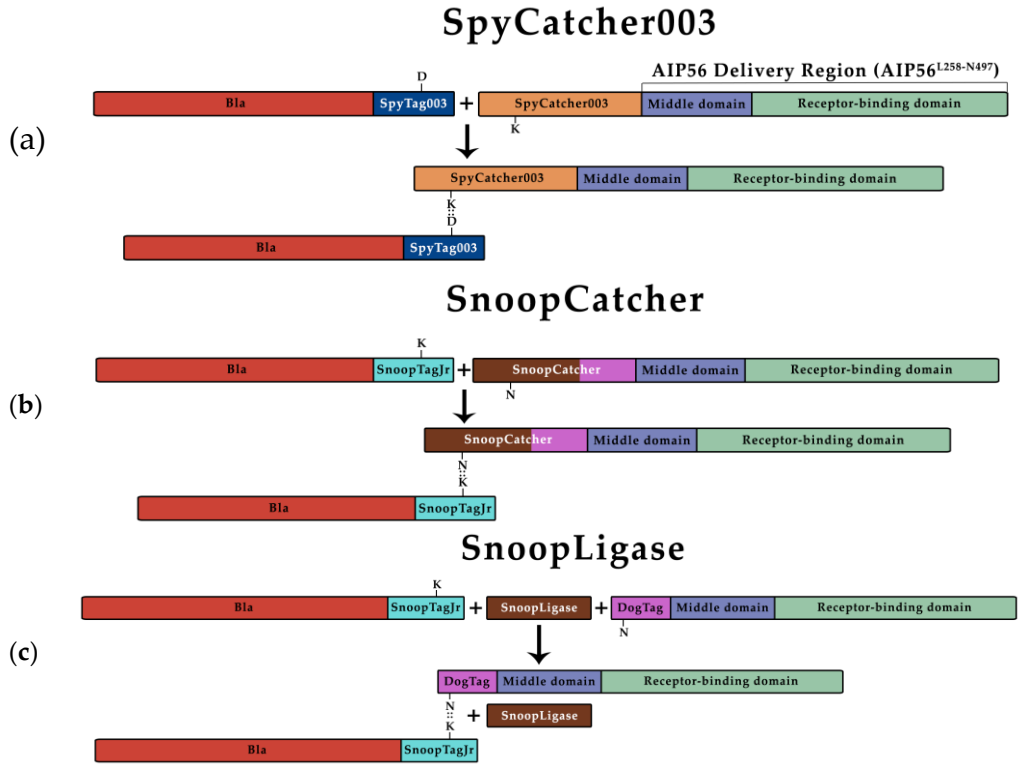

Figure 1. Schematic representation of protein-protein ligation reactions. All proteins were produced with the respective tags/protein partners, and incubated together to create Bla::AIP56$^{L258\text{-}N497}$ chimeras. **(a) SpyCatcher003.** D: Aspartate 556; K: Lysine 470. Both residues involved in the isopeptidic bond between SpyTag003 and SpyCatcher003. **(b) SnoopCatcher.** K: Lysine 742; N: Asparagine 854. Both residues involved in the isopeptidic bond between SnoopTagJr and SnoopCatcher. **(c) SnoopLigase.** K: Lysine 742; N: Asparagine 854. Both residues involved in the isopeptidic bond between SnoopTagJr and DogTag.

For the SpyCatcher-SpyTag reaction, Bla$^{L19\text{-}W286}$SpyTag003 was conjugated to SpyCatcher003AIP56$^{L258\text{-}N497}$ at 25 °C or 4 °C, using several molar ratios of the proteins. A 5:1 ratio resulted in the highest yield of Bla$^{L19\text{-}W286}$::SpyAIP56$^{L258\text{-}N497}$, with the reaction at 25 °C reaching nearly completion after 2 h of incubation, as shown by the depletion of SpyCatcher003AIP56$^{L258\text{-}N497}$ (Figure 2a and Figure S3).

Slightly different experimental conditions were tested for the SnoopCatcher-SnoopTagJr reaction. Specifically, Bla$^{L19\text{-}W286}$SnoopTagJr was conjugated to SnoopCatcherAIP56$^{L258\text{-}N497}$ at 25 °C or 17 °C. A 2:1 ratio resulted in a higher yield of Bla$^{L19\text{-}W286}$::SnoopAIP56$^{L258\text{-}N497}$, with the reaction performed at 25 °C, reaching nearly completion after 4 h of incubation, as shown by the depletion of SnoopCatcherAIP56$^{L258\text{-}N497}$ at this time point (Figure 2b and Figure S4).

The experimental conditions used for the DogTag-SnoopTagJr reaction were the following: Bla$^{L19\text{-}W286}$SnoopTagJr was mixed with DogTagAIP56$^{L258\text{-}N497}$ at different molar ratios in the presence of AviTagSnoopLigase and incubated at 25 °C, 17 °C or 4 °C. The best yield was obtained at 4 °C using a Bla$^{L19\text{-}W286}$SnoopTagJr:DogTagAIP56$^{L258\text{-}N497}$:AviTagSnoopLigase molar ratio of 2:2:1, respectively. Under these conditions, the reaction reached a plateau at the 24 h time point. Complete conversion of the reactive proteins into the chimera was not achieved, even after 48 h of incubation (Figure 2c and Figure S5).

 doi:10.20944/preprints202502.0284.v1

All the protein chimeras were purified (see materials and methods section) and tested for activity as described below.

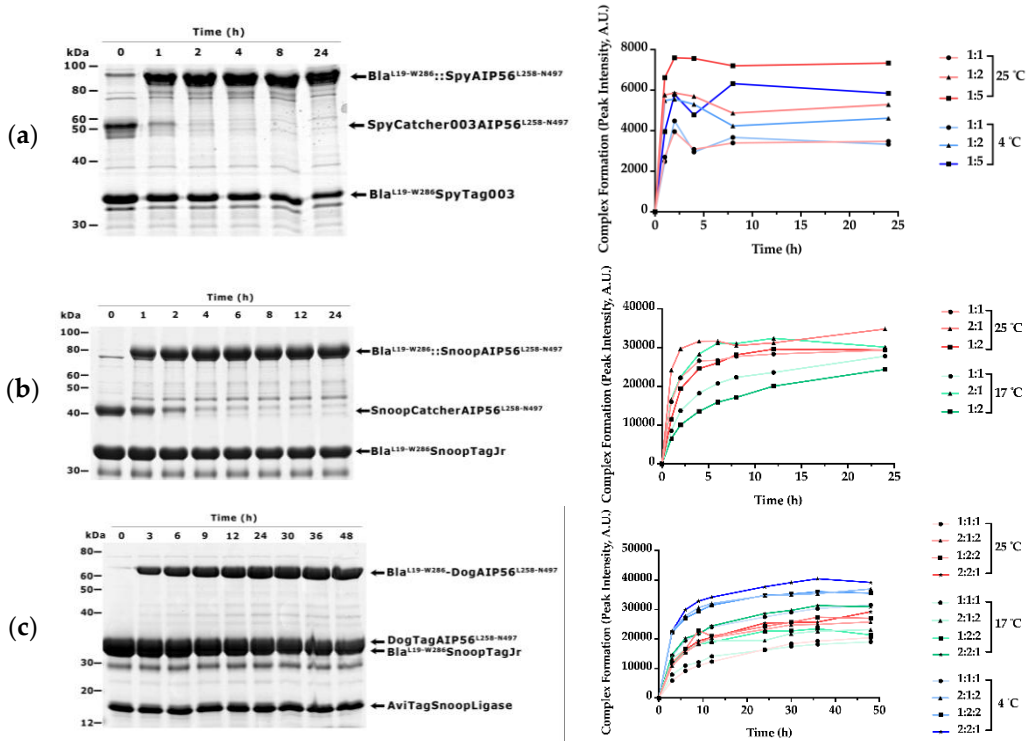

Figure 2. Time-course analyses of ligation reactions between β-lactamase and AIP56$^{L258\text{-}N497}$ (a) SDS-PAGE of the SpyCatcher003 reaction (left panel) and its quantification (right panel). The gel shows the results obtained with the best condition: 5:1 molar ratio of Bla$^{L19\text{-}W286}$SpyTag003 to SpyCatcher003AIP56$^{L258\text{-}N497}$ at 25 °C. Other reaction conditions are shown in Figure S3. Samples were analyzed by SDS-PAGE followed by Coomassie-blue R-250 staining. Bla$^{L19\text{-}W286}$SpyTag003 (32.6 kDa) reacted with SpyCatcher003AIP56$^{L258\text{-}N497}$ (41.3 kDa) to originate Bla$^{L19\text{-}W286}$::SpyAIP56$^{L258\text{-}N497}$ (73.9 kDa). (b) SDS-PAGE of the SnoopCatcher reaction (left panel) and its quantification (right panel). The gel shows the results obtained with the best condition: 2:1 molar ratio of Bla$^{L19\text{-}W286}$SnoopTagJr to SnoopCatcherAIP56$^{L258\text{-}N497}$ at 25 °C. Other experimental conditions are shown in Figure S4. Bla$^{L19\text{-}W286}$SnoopTagJr (31.8 kDa) reacted with SnoopCatcherAIP56$^{L258\text{-}N497}$ (41.2 kDa) to originate the Bla$^{L19\text{-}W286}$::SnoopAIP56$^{L258\text{-}N497}$ (73.0 kDa). (c) SnoopLigase reaction (left panel) and its quantification (right panel). The gel shows the best condition: 2:2:1 molar ratios of Bla$^{L19\text{-}W286}$SnoopTagJr to DogTagAIP56$^{L258\text{-}N497}$ to AviTagSnoopLigase at 4 °C. Other conditions are shown in Figure S5. Bla$^{L19\text{-}W286}$SnoopTagJr (31.8 kDa) reacted with DogTagAIP56$^{L258\text{-}N497}$ (31.1 kDa) catalyzed by AviTagSnoopLigase (15.4 kDa) to originate the Bla$^{L19\text{-}W286}$::DogAIP56$^{L258\text{-}N497}$ (62.9 kDa).

3.2. Bla$^{L19\text{-}W286}$::SpyAIP56$^{L258\text{-}N497}$, Bla$^{L19\text{-}W286}$::SnoopAIP56$^{L258\text{-}N497}$ and Bla$^{L19\text{-}W286}$::DogAIP56$^{L258\text{-}N497}$ + AviTagSnoopLigase Retain β-Lactamase Activity

To investigate whether the synthesized chimeras retain β-lactamase enzymatic activity, an *in vitro* nitrocefin colorimeric cleavage assay was conducted. Nitrocefin harbors a beta-lactam ring which is hydrolyzed by beta-lactamase. The hydrolysis reaction can be followed spectrophotometrically by measuring the increase of the absorbance at 486 nm [50].

In addition to the chemically synthesized chimeras, Bla$^{L19\text{-}W286}$SpyTag003, Bla$^{L19\text{-}W286}$SnoopTagJr and the genetic chimera Bla$^{L19\text{-}W286}$::AIP56$^{L258\text{-}N497}$ were also included in these assays, as controls. The progress curves obtained reveal that, all proteins tested possess β-lactamase activity (Figure 3). To compare activities among proteins, the slopes in the linear part of the graphs (the first 30 s of reaction) were calculated (Table 2). Bla$^{L19\text{-}W286}$::SnoopAIP56$^{L258\text{-}N497}$ and Bla$^{L19\text{-}W286}$SnoopTagJr displayed similar activities and were selected for further functional assays.

Preprints.org (www.preprints.org) | NOT PEER-REVIEWED | Posted: 5 February 2025 doi:10.20944/preprints202502.0284.v1

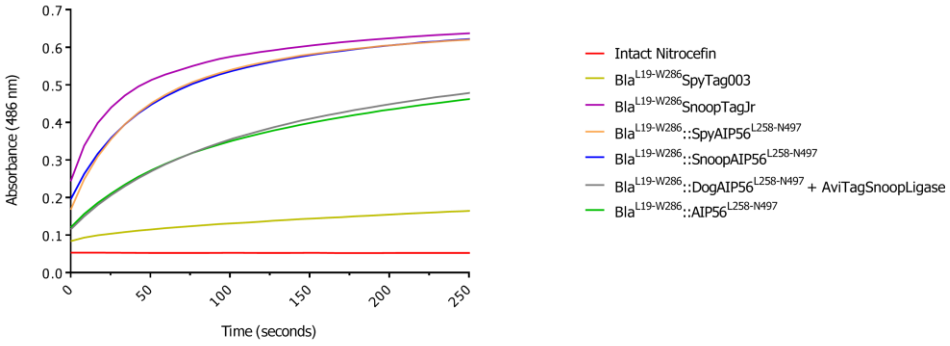

Figure 3. Nitrocefin hydrolysis by Bla$^{L19\text{-}W286}$-containing proteins. Bla$^{L19\text{-}W286}$::SnoopAIP56$^{L258\text{-}N497}$ and Bla$^{L19\text{-}W286}$SnoopTagJr have equivalent enzymatic activity. Each protein (5 nM) was incubated with 20 μM of nitrocefin and the absorbance was measured at 486 nm for 250 s.

Table 2. Relative activities of the Bla$^{L19\text{-}W286}$-containing proteins.

Protein	Slope (ΔAbs.min^{-1})
Bla$^{L19\text{-}W286}$SpyTag003	0.77 × 10^{-3}
Bla$^{L19\text{-}W286}$SnoopTagJr	7.66 × 10^{-3}
Bla$^{L19\text{-}W286}$::SpyAIP56$^{L258\text{-}N497}$	7.38 × 10^{-3}
Bla$^{L19\text{-}W286}$::SnoopAIP56$^{L258\text{-}N497}$	6.43 × 10^{-3}
Bla$^{L19\text{-}W286}$::DogAIP56$^{L258\text{-}N497}$+AviTagSnoopLigase	3.58 × 10^{-3}
Bla$^{L19\text{-}W286}$::AIP56$^{L258\text{-}N497}$	3.54 × 10^{-3}

3.3. Bla$^{L19\text{-}W286}$::SnoopAIP56$^{L258\text{-}N497}$ Transports β-Lactamase into the Cytosol of Macrophages

Toxin-mediated translocation of beta-lactamase across the cellular plasma membrane can be assessed by a Fluorescence Resonance Energy Transfer (FRET)-based assay [51]. The assay is based on a cell permeable substrate (CCF4-AM) that consists of a coumarin moiety connected by a β-lactam ring to fluorescein. Excitation of coumarin at 409 nm results in FRET to fluorescein with green fluorescence emission at 520 nm. Upon cleavage of the β-lactam ring by β-lactamase, FRET is disrupted and excitation of coumarin at 409 nm results in blue fluorescence emission at 447 nm. We have previously used this assay to show that a Bla$^{L19\text{-}W286}$::AIP56$^{L258\text{-}N497}$ chimera, obtained by genetic fusion, is able to deliver β-lactamase into the cytosol of mouse bone marrow-derived macrophages (mBMDM) [27,30]. Here, we used this assay to determine whether Bla$^{L19\text{-}W286}$::SnoopAIP56$^{L258\text{-}N497}$ is capable of delivering β-lactamase into the cytosol of mouse macrophages. Briefly, J774.A1 macrophages were loaded with CCF4-AM and were then either mock-treated or incubated with Bla$^{L19\text{-}W286}$::SnoopAIP56$^{L258\text{-}N497}$ or Bla$^{L19\text{-}W286}$SnoopTagJr, as a negative control. Cleavage of CCF4-AM was analyzed by fluorescence microscopy. As shown in Figure 4, Bla$^{L19\text{-}W286}$::SnoopAIP56$^{L258\text{-}N497}$ led to FRET disruption when compared to mock-treated cells ($p < 0.0001$) and cells treated with Bla$^{L19\text{-}W286}$SnoopTagJr ($p < 0.0001$). We conclude that Bla$^{L19\text{-}W286}$::SnoopAIP56$^{L258\text{-}N497}$ is capable of delivering β-lactamase into the cytosol.

 doi:10.20944/preprints202502.0284.v1

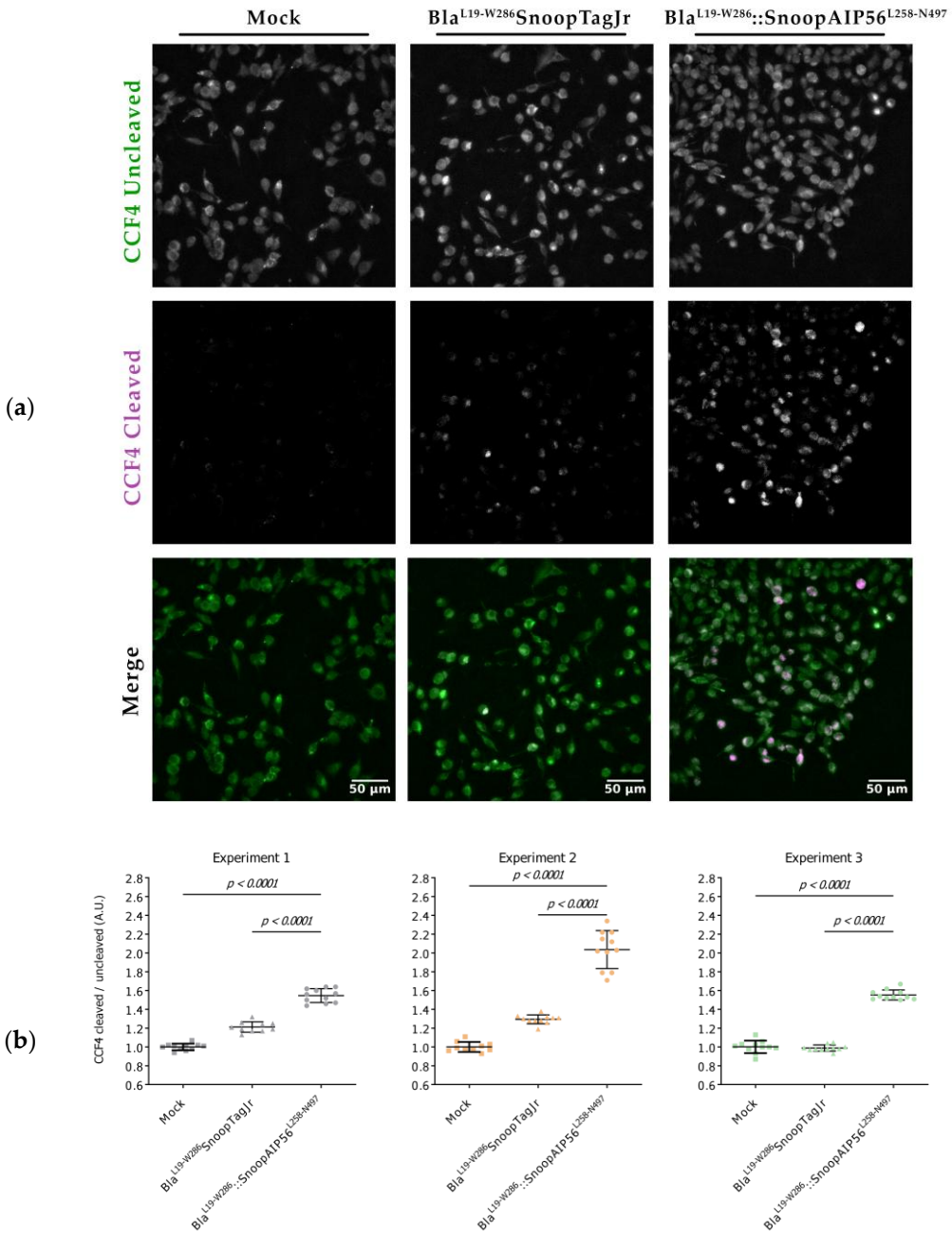

Figure 4. Bla$^{L19\text{-}W286}$::SnoopAIP56$^{L258\text{-}N497}$ delivers β-lactamase into the cytosol of J774.A1 murine macrophages. (a) Representative images of macrophages stained intracellularly with CCF4-AM. Cells were loaded with CCF4-AM before incubation with the indicated proteins for 15 min on ice followed by 45 min at 37 °C. Uncleaved and cleaved CCF4-AM signals were detected by fluorescence microscopy. Images shown correspond to representative microscopic fields obtained in one of three independent experiments. (b) Quantification of cleaved/uncleaved ratios of CCF4-AM. Cleaved/uncleaved ratios of CCF4-AM were obtained from three independent experiments. In each experiment, ratios were determined by quantifying at least 10 microscopic fields per condition and were normalized to the average ratio obtained from mock-treated cells. Groups comparisons were made using the Kruskal-Wallis test (Experiment 1, $p < 0.0001$; Experiment 2, $p < 0.0001$; Experiment 3, $p < 0.0001$). Pair-wise comparisons were performed using the Mann-Whitney test with Bonferroni correction (p-values are depicted in the graphs). Differences were considered significant when $p \leq 0.05$.

4. Discussion

A system capable of delivering large cargoes, such as proteins, to the cell cytosol would be of immense value in several areas of biotechnology and biomedicine, such as in infection, vaccination,

 doi:10.20944/preprints202502.0284.v1

immunomodulation and in anti-tumor activity. In this context, AB toxins rise as valid alternatives for the delivery of biological cargoes. In contrast to other delivery vectors [6–9], the structure and function mechanisms of many AB toxins are relatively well characterized, enabling their engineering to deliver different cargoes into the cytosol of target cells. In fact, several toxins are already being used as delivery tools with some success [11,16,52–54], although most of the toxin-cargo chimeras used to date have been produced by fusion at the genetic level. However, this approach is not always possible, due to low expression or solubility problems of the chimeras. An alternative to overcome this problem is to use chemical ligation strategies to connect the delivery moiety of the toxin to the pretended cargoes. Protein-protein fusion techniques mediated by sortase or by SpyCatcher-SpyTag have recently been applied to couple cargoes to toxins or to replace the receptor-binding domain of a toxin by a new ligand that confers a distinct cellular specificity [32,33,55].

We have previously shown that the middle and receptor-binding domains of AIP56 (AIP56$^{L258-N497}$) are sufficient to translocate β-lactamase from the endosomal compartment to the cytosol of macrophages by using chimeras produced through genetic engineering [27,30]. This, together with the fact that AIP56 targets mammalian APCs [29], supports the use of AIP56$^{L258-N497}$ as a platform for delivering antigens to APCs, similarly to what has been shown for CyaA, another AB toxin that also targets APCs [19,20]. However, contrary to CyaA and other AB toxins, which need to be previously activated by cleavage ("nicking") of a linker loop before triggering the translocation of their cargoes to the cytosol [56–59], AIP56 is ready to deliver its cargoes without any activation step [24,25]. Furthermore, in the case of CyA (1706 amino-acids long) antigens have been grafted to the catalytic domain of the full-length toxin [20], resulting in chimeras of substantial size, whereas in AIP56, the catalytic domain is replaced by the cargo, resulting in much smaller chimeras, with implications for production and immunogenicity. Moreover, CyaA inserts in the cell membrane, triggering potassium efflux as well as the formation of cation-specific pores that ultimately cause lysis of the APCs [20], posing limits to the dosage and compromising the immune response to the antigen. In contrast, AIP56 translocates only from endosomes [25] and its delivery domains can be used without harm to APCs.

A relevant aspect to consider for the success of a toxin-based vaccination platform is the existence of pre-acquired antigenicity to the toxin-vector or antigenicity acquired during vaccination, which may prevent its use, especially when multiple inoculations are required. Although mutation of immunogenic epitopes or administration of immunosuppressants have been used in protein-based therapies to solve the antigenicity problem [2, 3], mutating the right epitopes can be challenging and immunosuppressants have unwanted side effects and should be avoided when the objective is to induce an immune response against an antigen. Although bacterial toxins may be highly immunogenic by nature [60–63], the producing agent of AIP56, *Photobacterium damselae* subsp. *piscicida*, is a well-recognized fish pathogen that does not infect mammals, rendering neutralization of AIP56 by antibodies generated during previous contact with this pathogen unlikely. Even if it were to occur, the use of protein-protein fusion techniques would allow quick coupling of antigens (or drugs) to delivery platforms based on different toxins prepared in advance for this purpose.

In addition to the many AB toxins already studied, there are several uncharacterized toxins in different species of prokaryotes and eukaryotes whose three-dimensional structures predicted by AlphaFold are identical to the crystallographic structure of AIP56 (AIP56-like toxins) or contain a domain similar to the receptor-binding domain of AIP56 (AIP56-related toxins) [27]. Moreover, rabbit and rat antiserum against AIP56 do not cross-react with some of these toxins (Figure S6), suggesting that the middle and receptor-binding domains of those toxins could also be used as a viable and/or complementary alternative to the AIP56-based platform.

In this work, we successfully obtained chimeras of AIP56$^{L258-N497}$ with Bla$^{L19-W286}$ using SpyCatcher003, SnoopCatcher and SnoopLigase ligation strategies. More importantly, when we incubated mouse J774.A1 macrophages with Bla$^{L19-W286}$::SnoopAIP56$^{L258-N497}$, the chimera was able to deliver β-lactamase to the cytosol of these cells. These results thus indicate that protein-protein fusion strategies, although more laborious, are feasible and valid alternatives to genetically fusion strategies, particularly when the latter approach is unsuitable. We anticipate that by extending these strategies

 doi:10.20944/preprints202502.0284.v1

to other AB toxins, including a range of toxins homologous to AIP56, it will be possible to create a "toolbox" with functionally equivalent but antigenically different interchangeable delivery vehicles ready to couple different antigens.

Supplementary Materials: The following supporting information can be downloaded at: www.mdpi.com/xxx/s1, Figure S1: Cartoon representation of the SpyCatcher, SnoopCatcher and SnoopLigase fusion systems; Figure S2: SDS-PAGE profile of the purified recombinant proteins and protein fusions used in this work; Figure S3: Time-course analysis of $Bla^{L19\text{-}W286}$SpyTag003 + SpyCatcher003$AIP56^{L258\text{-}N497}$ protein fusion; Figure S4: Time-course analysis of $Bla^{L19\text{-}W286}$SnoopTagJr + SnoopCatcher$AIP56^{L258\text{-}N497}$ protein fusion at different protein ratios and temperatures; Figure S5: Time-course analysis of $Bla^{L19\text{-}W286}$SnoopTagJr + DogTag$AIP56^{L258\text{-}N497}$ protein fusion at different protein ratios and temperatures; Figure S6: AIP56-like and AIP56-related toxins are not immunogenically identical; Source Data.

Author Contributions: B.P., A.C.M., A.d.V. and N.M.S.S. conceived the study and the experiments; B.P. and A.C.M. performed all the experimental procedures; B.P., A.C.M., A.d.V., J.E.A. and N.M.S.S. analyzed the results; B.P. prepared the figures; P.O. performed statistical analysis; B.P., and N.M.S.S. wrote the manuscript with contribution by A.C.M., A.d.V. and J.E.A.; All authors reviewed and approved the final version of the manuscript.

Funding: This work was supported by National funds through FCT under the project UIDB/04293/2020 and by FEDER funds through Programa Operacional Factores de Competitividade – COMPETE and by national funds through FCT – Fundação para a Ciência e a Tecnologia under the project PTDC/BIA-MIC/29910/2017 to N.M.S.S. A.d.V. was funded by Portuguese national funds through the FCT and, when eligible, by COMPETE 2020 FEDER funds, under the Scientific Employment Stimulus–Individual Call 2021.02251.CEECIND/CP1663/CT0016. B.P. was funded by FCT – Fundação para a Ciência e a Tecnologia (2020.07395.BD).

Data Availability Statement: The original contributions presented in this study are included in the article/supplementary material. Further inquiries can be directed to the corresponding author(s).

Acknowledgments: The authors acknowledge the support of the i3S Scientific Platform Advanced Light Microscopy, a site of PPBI Euro-Bioimaging Node and Biochemical and Biophysical Technologies Scientific Platform. A special thanks to Constance Kowal, Inês Lua Freitas and Dr. Johnny Lisboa for the contributions in this work, and Dr. Dimitri Panagiotis Papatheodorou for providing plasmid p327.

Conflicts of Interest: The authors declare no conflicts of interest.

References

1. 1. Biopharmaceuticals Market Size Report, 2022-2027 Available online: https://www.industryarc.com/Report/9586/biopharmaceutical-market.html (accessed on 10 July 2024).
2. 2. Fosgerau, K.; Hoffmann, T. Peptide Therapeutics: Current Status and Future Directions. *Drug Discov. Today* **2015**, *20*, 122–128.
3. 3. Basak, D.; Arrighi, S.; Darwiche, Y.; Deb, S. Comparison of Anticancer Drug Toxicities: Paradigm Shift in Adverse Effect Profile. *Life* **2022**, *12*, 48.
4. 4. Reinhard, K.; Rengstl, B.; Oehm, P.; Michel, K.; Billmeier, A.; Hayduk, N.; Klein, O.; Kuna, K.; Ouchan, Y.; Wöll, S.; et al. An RNA Vaccine Drives Expansion and Efficacy of Claudin-CAR-T Cells against Solid Tumors. *Science* **2020**, *367*, 446–453.
5. 5. Dai, L.; Gao, G.F. Viral Targets for Vaccines against COVID-19. *Nat. Rev. Immunol.* **2021**, *21*, 73–82.
6. 6. Zepeda-Cervantes, J.; Ramírez-Jarquín, J.O.; Vaca, L. Interaction Between Virus-Like Particles (VLPs) and Pattern Recognition Receptors (PRRs) From Dendritic Cells (DCs): Toward Better Engineering of VLPs. *Front. Immunol.* **2020**, *11*.
7. 7. Khan, M.M.; Filipczak, N.; Torchilin, V.P. Cell Penetrating Peptides: A Versatile Vector for Co-Delivery of Drug and Genes in Cancer. *J. Controlled Release* **2021**, *330*, 1220–1228.
8. 8. Gessner, I.; Klimpel, A.; Klußmann, M.; Neundorf, I.; Mathur, S. Interdependence of Charge and Secondary Structure on Cellular Uptake of Cell Penetrating Peptide Functionalized Silica Nanoparticles. *Nanoscale Adv.* **2020**, *2*, 453–462.
9. 9. Yetisgin, A.A.; Cetinel, S.; Zuvin, M.; Kosar, A.; Kutlu, O. Therapeutic Nanoparticles and Their Targeted Delivery Applications. *Molecules* **2020**, *25*, 2193.

10. 10. Beilhartz, G.L.; Sugiman-Marangos, S.N.; Melnyk, R.A. Repurposing Bacterial Toxins for Intracellular Delivery of Therapeutic Proteins. *Biochem. Pharmacol.* **2017**, *142*, 13–20.
11. 11. Piot, N.; van der Goot, F.G.; Sergeeva, O.A. Harnessing the Membrane Translocation Properties of AB Toxins for Therapeutic Applications. *Toxins* **2021**, *13*, 36.
12. 12. Falnes, P.O.; Sandvig, K. Penetration of Protein Toxins into Cells. *Curr. Opin. Cell Biol.* **2000**, *12*, 407–413.
13. 13. Geny, B.; Popoff, M.R. Bacterial Protein Toxins and Lipids: Role in Toxin Targeting and Activity. *Biol. Cell* **2006**, *98*, 633–651.
14. 14. Geny, B.; Popoff, M.R. Bacterial Protein Toxins and Lipids: Pore Formation or Toxin Entry into Cells. *Biol. Cell* **2006**, *98*, 667–678.
15. 15. Márquez-López, A.; Fanarraga, M.L. AB Toxins as High-Affinity Ligands for Cell Targeting in Cancer Therapy. *Int. J. Mol. Sci.* **2023**, *24*, 11227.
16. 16. Odumosu, O.; Nicholas, D.; Yano, H.; Langridge, W. AB Toxins: A Paradigm Switch from Deadly to Desirable. *Toxins* **2010**, *2*, 1612–1645.
17. 17. Eriksson, K.; Fredriksson, M.; Nordström, I.; Holmgren, J. Cholera Toxin and Its B Subunit Promote Dendritic Cell Vaccination with Different Influences on Th1 and Th2 Development. *Infect. Immun.* **2003**, *71*, 1740–1747.
18. 18. Batisse, C.; Dransart, E.; Ait Sarkouh, R.; Brulle, L.; Bai, S.-K.; Godefroy, S.; Johannes, L.; Schmidt, F. A New Delivery System for Auristatin in STxB-Drug Conjugate Therapy. *Eur. J. Med. Chem.* **2015**, *95*, 483–491.
19. 19. Ladant, D. Bioengineering of *Bordetella Pertussis* Adenylate Cyclase Toxin for Vaccine Development and Other Biotechnological Purposes. *Toxins* **2021**, *13*, 83.
20. 20. Chenal, A.; Ladant, D. Bioengineering of *Bordetella Pertussis* Adenylate Cyclase Toxin for Antigen-Delivery and Immunotherapy. *Toxins* **2018**, *10*, 302.
21. 21. Falahatgar, D.; Farajnia, S.; Zarghami, N.; Tanomand, A.; Ahdi Khosroshahi, S.; Akbari, B.; Farajnia, H. Expression and Evaluation of HuscFv Antibody -PE40 Immunotoxin for Target Therapy of EGFR-Overexpressing Cancers. *Iran. J. Biotechnol.* **2018**, *16*, 241–247.
22. 22. Weldon, J.E.; Xiang, L.; Chertov, O.; Margulies, I.; Kreitman, R.J.; FitzGerald, D.J.; Pastan, I. A Protease-Resistant Immunotoxin against CD22 with Greatly Increased Activity against CLL and Diminished Animal Toxicity. *Blood* **2009**, *113*, 3792–3800.
23. 23. Do Vale, A.; Silva, M.T.; Santos, N.M.S. dos; Nascimento, D.S.; Reis-Rodrigues, P.; Costa-Ramos, C.; Ellis, A.E.; Azevedo, J.E. AIP56, a Novel Plasmid-Encoded Virulence Factor of Photobacterium Damselae Subsp. Piscicida with Apoptogenic Activity against Sea Bass Macrophages and Neutrophils. *Mol. Microbiol.* **2005**, *58*, 1025–1038.
24. 24. Silva, D.S.; Pereira, L.M.G.; Moreira, A.R.; Ferreira-da-Silva, F.; Brito, R.M.; Faria, T.Q.; Zornetta, I.; Montecucco, C.; Oliveira, P.; Azevedo, J.E.; et al. The Apoptogenic Toxin AIP56 Is a Metalloprotease A-B Toxin That Cleaves NF-Kb P65. *PLOS Pathog.* **2013**, *9*, e1003128.
25. 25. Pereira, L.M.G.; Pinto, R.D.; Silva, D.S.; Moreira, A.R.; Beitzinger, C.; Oliveira, P.; Sampaio, P.; Benz, R.; Azevedo, J.E.; dos Santos, N.M.S.; et al. Intracellular Trafficking of AIP56, an NF-κB-Cleaving Toxin from Photobacterium Damselae Subsp. Piscicida. *Infect. Immun.* **2014**, *82*, 5270–5285.
26. 26. Do Vale, A.; Pereira, C.; R. Osorio, C.; MS dos Santos, N. The Apoptogenic Toxin AIP56 Is Secreted by the Type II Secretion System of *Photobacterium Damselae* Subsp. *Piscicida*. *Toxins* **2017**, *9*, 368.
27. 27. Lisboa, J.; Pereira, C.; Pinto, R.D.; Rodrigues, I.S.; Pereira, L.M.G.; Pinheiro, B.; Oliveira, P.; Pereira, P.J.B.; Azevedo, J.E.; Durand, D.; et al. Unconventional Structure and Mechanisms for Membrane Interaction and Translocation of the NF-κB-Targeting Toxin AIP56. *Nat. Commun.* **2023**, *14*, 7431.
28. 28. Pereira, C.; Rodrigues, I.S.; Pereira, L.M.G.; Lisboa, J.; Pinto, R.D.; Araújo, L.; Oliveira, P.; Benz, R.; Santos, N.M.S. dos; Vale, A. do Role of AIP56 Disulphide Bond and Its Reduction by Cytosolic Redox Systems for Efficient Intoxication. *Cell. Microbiol.* **2019**, *0*, e13109.
29. 29. Freitas, I.L.; Macedo, F.; Oliveira, L.; Oliveria, P.; do Vale, A.; dos Santos, N.M.S. AIP56, an AB Toxin Secreted by Photobacterium Damselae Subsp. Piscicida, Has Tropism for Myeloid Cells. *Front. Immunol.* **2024**, *15*.

 doi:10.20944/preprints202502.0284.v1

30. 30. Rodrigues, I.S.; Pereira, L.M.G.; Lisboa, J.; Pereira, C.; Oliveira, P.; Santos, N.M.S. dos; Vale, A. do Involvement of Hsp90 and Cyclophilins in Intoxication by AIP56, a Metalloprotease Toxin from Photobacterium Damselae Subsp. Piscicida. *Sci. Rep.* **2019**, *9*, 9019.
31. 31. Rabideau, A.E.; Pentelute, B.L. Delivery of Non-Native Cargo into Mammalian Cells Using Anthrax Lethal Toxin. *ACS Chem. Biol.* **2016**, *11*, 1490–1501.
32. 32. Miyashita, S.-I.; Zhang, J.; Zhang, S.; Shoemaker, C.B.; Dong, M. Delivery of Single-Domain Antibodies into Neurons Using a Chimeric Toxin–Based Platform Is Therapeutic in Mouse Models of Botulism. *Sci. Transl. Med.* **2021**, *13*.
33. 33. Park, S.G.; Lee, H.B.; Kang, S. Development of Plug-and-Deliverable Intracellular Protein Delivery Platforms Based on Botulinum Neurotoxin. *Int. J. Biol. Macromol.* **2024**, *261*, 129622.
34. 34. Zakeri, B.; Fierer, J.O.; Celik, E.; Chittock, E.C.; Schwarz-Linek, U.; Moy, V.T.; Howarth, M. Peptide Tag Forming a Rapid Covalent Bond to a Protein, through Engineering a Bacterial Adhesin. *Proc. Natl. Acad. Sci. U. S. A.* **2012**, *109*, E690–E697.
35. 35. Li, L.; Fierer, J.O.; Rapoport, T.A.; Howarth, M. Structural Analysis and Optimization of the Covalent Association between SpyCatcher and a Peptide Tag. *J. Mol. Biol.* **2014**, *426*, 309–317.
36. 36. Veggiani, G.; Nakamura, T.; Brenner, M.D.; Gayet, R.V.; Yan, J.; Robinson, C.V.; Howarth, M. Programmable Polyproteams Built Using Twin Peptide Superglues. *Proc. Natl. Acad. Sci.* **2016**, *113*, 1202–1207.
37. 37. Izoré, T.; Contreras-Martel, C.; El Mortaji, L.; Manzano, C.; Terrasse, R.; Vernet, T.; Di Guilmi, A.M.; Dessen, A. Structural Basis of Host Cell Recognition by the Pilus Adhesin from *Streptococcus Pneumoniae*. *Structure* **2010**, *18*, 106–115.
38. 38. Buldun, C.M.; Jean, J.X.; Bedford, M.R.; Howarth, M. SnoopLigase Catalyzes Peptide-Peptide Locking and Enables Solid-Phase Conjugate Isolation. *J. Am. Chem. Soc.* **2018**, *140*, 3008–3018.
39. 39. Li, L.; Fierer, J.O.; Rapoport, T.A.; Howarth, M. Structural Analysis and Optimization of the Covalent Association between SpyCatcher and a Peptide Tag. *J. Mol. Biol.* **2014**, *426*, 309–317.
40. 40. Keeble, A.H.; Banerjee, A.; Ferla, M.P.; Reddington, S.C.; Anuar, I.N.A.K.; Howarth, M. Evolving Accelerated Amidation by SpyTag/SpyCatcher to Analyze Membrane Dynamics. *Angew. Chem. Int. Ed Engl.* **2017**, *56*, 16521–16525.
41. 41. Keeble, A.H.; Turkki, P.; Stokes, S.; Khairil Anuar, I.N.A.; Rahikainen, R.; Hytönen, V.P.; Howarth, M. Approaching Infinite Affinity through Engineering of Peptide–Protein Interaction. *Proc. Natl. Acad. Sci.* **2019**, *116*, 26523–26533.
42. 42. Keeble, A.H.; Wood, D.P.; Howarth, M. Design and Evolution of Enhanced Peptide-Peptide Ligation for Modular Transglutaminase Assembly. *Bioconjug. Chem.* **2023**, *34*, 1019–1036.
43. 43. Laemmli, U.K. Cleavage of Structural Proteins during the Assembly of the Head of Bacteriophage T4. *Nature* **1970**, *227*, 680–685.
44. 44. Schindelin, J.; Arganda-Carreras, I.; Frise, E.; Kaynig, V.; Longair, M.; Pietzsch, T.; Preibisch, S.; Rueden, C.; Saalfeld, S.; Schmid, B.; et al. Fiji: An Open-Source Platform for Biological-Image Analysis. *Nat. Methods* **2012**, *9*, 676–682.
45. 45. Kaderabkova, N.; Bharathwaj, M.; Furniss, R.C.D.; Gonzalez, D.; Palmer, T.; Mavridou, D.A.I. The Biogenesis of β-Lactamase Enzymes. *Microbiology* **2022**, *168*, 001217.
46. 46. Zlokarnik, G. Fusions to Beta-Lactamase as a Reporter for Gene Expression in Live Mammalian Cells. *Methods Enzymol.* **2000**, *326*, 221–244.
47. 47. Moore, J.T.; Davis, S.T.; Dev, I.K. The Development of β-Lactamase as a Highly Versatile Genetic Reporter for Eukaryotic Cells. *Anal. Biochem.* **1997**, *247*, 203–209.
48. 48. Zlokarnik, G.; Negulescu, P.A.; Knapp, T.E.; Mere, L.; Burres, N.; Feng, L.; Whitney, M.; Roemer, K.; Tsien, R.Y. Quantitation of Transcription and Clonal Selection of Single Living Cells with β-Lactamase as Reporter. *Science* **1998**, *279*, 84–88.
49. 49. Campbell, R.E. Realization of β-Lactamase as a Versatile Fluorogenic Reporter. *Trends Biotechnol.* **2004**, *22*, 208–211.

50. 50. O'Callaghan, C.H.; Morris, A.; Kirby, S.M.; Shingler, A.H. Novel Method for Detection of β-Lactamases by Using a Chromogenic Cephalosporin Substrate. *Antimicrob. Agents Chemother.* **1972**, *1*, 283–288.
51. 51. Zuverink, M.; Barbieri, J.T. From GFP to β-Lactamase: Advancing Intact Cell Imaging for Toxins and Effectors. *Pathog. Dis.* **2015**, *73*.
52. 52. Akbari, B.; Farajnia, S.; Ahdi Khosroshahi, S.; Safari, F.; Yousefi, M.; Dariushnejad, H.; Rahbarnia, L. Immunotoxins in Cancer Therapy: Review and Update. *Int. Rev. Immunol.* **2017**, *36*, 207–219.
53. 53. Beddoe, T.; Paton, A.W.; Le Nours, J.; Rossjohn, J.; Paton, J.C. Structure, Biological Functions and Applications of the AB5 Toxins. *Trends Biochem. Sci.* **2010**, *35*, 411–418.
54. 54. Kenworthy, A.K.; Schmieder, S.S.; Raghunathan, K.; Tiwari, A.; Wang, T.; Kelly, C.V.; Lencer, W.I. Cholera Toxin as a Probe for Membrane Biology. *Toxins* **2021**, *13*, 543.
55. 55. Park, S.; Choi, B.; Bae, Y.; Lee, Y.G.; Park, S.; Chae, Y.; Kang, S. Selective and Effective Cancer Treatments Using Target-Switchable Intracellular Bacterial Toxin Delivery Systems. *Adv. Ther.* **2020**, *3*, 2000043.
56. 56. Wernick, N.L.B.; Chinnapen, D.J.-F.; Cho, J.A.; Lencer, W.I. Cholera Toxin: An Intracellular Journey into the Cytosol by Way of the Endoplasmic Reticulum. *Toxins* **2010**, *2*, 310–325.
57. 57. Young, J.A.T.; Collier, R.J. Anthrax Toxin: Receptor Binding, Internalization, Pore Formation, and Translocation. *Annu. Rev. Biochem.* **2007**, *76*, 243–265.
58. 58. Gordon, V.M.; Leppla, S.H. Proteolytic Activation of Bacterial Toxins: Role of Bacterial and Host Cell Proteases. *Infect. Immun.* **1994**, *62*, 333–340.
59. 59. Uribe, K.B.; Etxebarria, A.; Martín, C.; Ostolaza, H. Calpain-Mediated Processing of Adenylate Cyclase Toxin Generates a Cytosolic Soluble Catalytically Active N-Terminal Domain. *PLoS ONE* **2013**, *8*, e67648.
60. 60. Carr, W.W.; Jain, N.; Sublett, J.W. Immunogenicity of Botulinum Toxin Formulations: Potential Therapeutic Implications. *Adv. Ther.* **2021**, *38*, 5046–5064.
61. 61. Yu, R.; Fang, T.; Liu, S.; Song, X.; Yu, C.; Li, J.; Fu, L.; Hou, L.; Xu, J.; Chen, W. Comparative Immunogenicity of the Tetanus Toxoid and Recombinant Tetanus Vaccines in Mice, Rats, and Cynomolgus Monkeys. *Toxins* **2016**, *8*, 194.
62. 62. Elson, C.O. Cholera Toxin and Its Subunits as Potential Oral Adjuvants. In Proceedings of the New Strategies for Oral Immunization; Mestecky, J., McGhee, J.R., Eds.; Springer: Berlin, Heidelberg, 1989; pp. 29–33.
63. 63. Mazor, R.; Pastan, I. Immunogenicity of Immunotoxins Containing *Pseudomonas* Exotoxin A: Causes, Consequences, and Mitigation. *Front. Immunol.* **2020**, *11*.